Quantum dots: few-body, low-dimensional systems

1995 J. Phys.: Condens. Matter 7 965

(http://iopscience.iop.org/0953-8984/7/6/005)

J. Phys.: Condens. Matter 7 (1995) 965–989. Printed in the UK

REVIEW ARTICLE

Quantum dots: few-body, low-dimensional systems

Neil F Johnson
Department of Physics, Oxford University, Oxford OX1 3PU, UK

Received 24 June 1994, in final form 1 November 1994

Abstract. Quantum dots are examples of nanostructures which are attracting much interest in the fields of both pure and applied physics. The smallest dots currently being fabricated contain $N < 10$ interacting electrons and have an effective dimensionality $d \leqslant 3$. The measurement and interpretation of the energy spectra associated with such few-particle quantum dots represents a considerable experimental and theoretical challenge. The single-electron confinement energy, the cyclotron energy for moderate magnetic fields and the electron–electron interaction energy can be of similar magnitude and may therefore be equally important in determining the few-electron energy levels. In addition the energy spectrum is likely to be strongly N dependent for such small N. Here we review the results to date for few-particle quantum dots ($N < 10$). We discuss the extent to which theoretical predictions emerging from detailed numerical calculations can be reproduced using analytically solvable microscopic models, and the extent to which both are consistent with recent experimental results.

1. Introduction

In recent years there has been much excitement surrounding the possible applications of ultrasmall systems on the 10–1000 Å length scale in the areas of electronics and optoelectronics [1]. Structures whose dimensions are of this length scale are often called nanostructures. The basic technological motivation is that smaller components should be faster and may also dissipate less heat. There are also the added features that at small enough length scales, quantum-mechanical effects will become important and that with few enough particles (e.g. $N < 10$), the properties should be strongly N dependent. Apart from their potential use as novel devices, such systems are interesting from a fundamental physics viewpoint. Recent advances in materials processing, electron and x-ray lithography have opened up the possibility of fabricating artificial nanostructures using a 'top-down' approach starting from a semiconductor heterostructure containing a quasi-two-dimensional electron gas [2–7]. Simultaneously, the present capability of manipulating single atoms using an STM (scanning tunnelling microscope) combined with recent progress in molecular synthesis have opened up the possibility of constructing molecular-scale devices using a 'bottom-up' approach. It has even been suggested that such molecular machinery could be self-assembling [8]. In addition there are many naturally occurring nanostructures such as C_{60} buckyball, porous silicon tubules and a wide variety of biological structures. Interest in nanostructures has therefore spanned the fields of engineering, chemistry, materials science, molecular biology and physics.

Because of their finite size nanostructures contain a finite number of electrons. If the number of electrons is large, it is reasonable to expect that their electronic properties may be qualitatively described by appealing to known properties of the infinite ($N \to \infty$) electron gas. However for small numbers of electrons (e.g. $N < 10$) the electronic properties of

0953-8984/95/060965+25$19.50

the system are likely to be strongly N dependent, particularly in the quantum-mechanical regime. The large variation in chemistry of the first few elements in the atomic periodic table suggests that this will be the case. Furthermore, according to the geometrical shape of the nanostructure, the confinement length scales in the three spatial directions in the nanostructure (L_x, L_y and L_z) can be quite different. Within a simple particle-in-a-box picture the single-particle energy-level spacing $\Delta E \sim L^{-2}$; it follows that for $L_x \gg L_y, L_z$ the electrons will be stuck in the lowest y, z subbands hence freezing out the y, z degrees of freedom. The nanostructure is now quasi-one dimensional in that the electrons only have significant freedom along the x-direction. Similarly if $L_x \sim L_y \gg L_z$ the nanostructure is quasi-two dimensional; if $L_x \sim L_y \sim L_z$ the nanostructure is quasi-three dimensional. The finite particle number N and reduced effective dimensionality $d \leqslant 3$ in nanostructures opens up a new research area in the traditionally large-N field of condensed-matter physics: the study of low-dimensional, few-body systems.

In the field of semiconductor physics, nanostructures with confinement in all three directions represent a logical progression from quantum wells, where the electrons are free to move in two directions, and quantum wires, where the electrons can only move in one. Semiconductor nanostructures where the electrons have no free directions might reasonably therefore be called quantum boxes or *quantum dots*. The connotation is that the electron wavelength is of the same length scale as the confinement so that quantum effects are important. In practice, however, nanometre-scale semiconductor structures are often called quantum dots irrespective of whether they actually exhibit quantum-mechanical confinement effects or not. Given that the trend in the experimental semiconductor nanostructure field is toward ever smaller systems (and hence smaller N), and given that the quantum-mechanical, few-body problem has relevance for a wide range of both artificial and natural nanostructures, we will limit this review of quantum dots to systems containing relatively few particles ($N < 10$) and with wavefunction confinement in all three spatial directions, thereby exhibiting a discrete, few-body energy spectrum. This classification is consistent with the widely held view of quantum dots as 'artificial atoms' [7]. As discussed above, such quantum dots can be effectively one, two or three dimensional (i.e. $d \leqslant 3$) according to the relative confinement lengths. The energy spectrum of the few-electron, semiconductor quantum dot is expected to be extremely rich since the single-electron confinement energy, the cyclotron energy for modest fields and the electron–electron interaction energy can all be of similar magnitude (typically a few millielectronvolts); none of the energy scales can *a priori* be thought of as a small perturbation. The energy spectrum is also likely to be strongly N dependent for $N < 10$.

This review discusses the various experimental and theoretical results which have been obtained for the few-particle ($N < 10$), low-dimensional ($d \leqslant 3$) quantum dot. Given the inherent difficulties related to experimental fabrication and investigation of quantum dots containing such few electrons, most work to date in the $N < 10$ regime has been theoretical. Consequently this review focuses on theoretical results, although connection to existing experimental data is made wherever possible. With the rapid progress in device fabrication techniques, it may become possible to experimentally test many of the theoretical predictions within the next few years. In fact the theoretical problem of N particles in d dimensions is of interest in its own right since it can serve as a cluster calculation for many-particle systems. Of particular interest is the investigation of small-N precursors of exotic many-body states such as fractional-quantum-Hall-effect (FQHE) states and Wigner solids. Given the rich phenomena that can occur in a two-dimensional electron gas, it is natural to expect related effects in a few-electron system such as a quantum dot.

Most of the theoretical work to date on the energy spectra of few-electron quantum dots

has been numerical and fairly computationally intensive. The results of these calculations have been reported for specific values of the dot parameters and/or N. In practice quantum dots can be fabricated with nominal parameters chosen from a wide range of possible values; in addition, there are uncertainties in the actual parameter values for a given dot sample (e.g. the geometric lengths of the dot do not usually correspond to the confinement lengths). To aid in the interpretation of experimental data, it might therefore be useful to gain more insight into *trends* in behaviour of the N-electron energy spectrum at the possible expense of quantitative accuracy for a particular set of dot parameters. For example, it would be useful to have approximate expressions for the N-particle energy spectrum from which characteristic features for a given N (i.e. a 'fingerprint') could be deduced. With this motivation, we will highlight throughout this review the extent to which the physics emerging from numerical calculations can be reproduced using analytically solvable microscopic model Hamiltonians. The latter provide closed-form expressions for the few-electron energy spectra as a function of the dot parameters, thereby providing insight into the complicated competition between the confinement, electron–electron-interaction and cyclotron energies.

The paper is arranged as follows. Section 2 discusses the various fabrication techniques and experimental investigations of the few-electron quantum dot. Section 3 reviews the various theoretical approaches that have been reported. Section 4.1 discusses the quasi-one-dimensional quantum dot (1DQD) where $L_x \gg L_y, L_z$. Section 4.2 reviews results for quasi-two-dimensional quantum dots (2DQD). Section 4.3 considers three-dimensional dots (3DQD). Finally section 5 discusses the properties of coupled, few-particle quantum dots.

2. Experimental background

Quantum dots have been fabricated using a variety of techniques. Several of these techniques centre around additional lateral confinement of a high-mobility, two-dimensional electron gas formed in a semiconductor (e.g. GaAs) heterostructure [4]. One method of obtaining this lateral confinement uses a mask of resist material defined on top of the heterostructure; this resist is a polymer which is either sensitive to electrons or x-rays depending on the type of lithography which is then performed to define the dot. The dot structure can also be defined using the profile of the resist material as a mask for etching. Another method of obtaining lateral confinement in the two-dimensional electron gas is to lay down a metallic gate on top of the photoresist structure; when biased negatively the gate will deplete electrons underneath which are closest to it, thereby defining the dot [4]. Similarly, electrodes defining the geometric size of the dot can be placed directly on top of the heterostructure with a gate below [7]; varying the voltage on these electrodes defines the quantum-dot region in the two-dimensional electron gas immediately underneath [7]. In each case, the geometric size of the quantum-dot structure tends to be larger than the actual electrostatic confinement diameter felt by the electrons. Alternative methods of quantum dot fabrication include the natural formation of microcrystallites from solution (e.g. CdS). For a detailed review of microcrystallites, we refer to [9]. There has also been a recent report of naturally occurring semiconductor quantum dots at the interface in a quantum-well structure [10]. In addition circular quantum-dot structures called quantum corrals have been constructed by positioning iron adatoms on a copper surface using an STM [11].

There are a large number of publications reporting transport and optical measurements on semiconductor quantum dots (see, for example, [5], [7] and [12]–[22]). Much experimental work has focused on large-N dots (i.e. $N \geqslant 20$). In this regime, the energy required to

add an extra electron to the dot can, to a good approximation, be separated into a large classical charging energy E_C which includes the effects of electron–electron interactions on the dot, plus a smaller energy-level-spacing term ΔE reflecting the separation between single-electron confinement levels on the dot. Although this approximation fails to treat the electron–electron interaction and the single-electron confinement on the same quantum-mechanical footing, it works well for large dots ($N \geqslant 20$) since large N implies large electrostatic energy E_C but small ΔE since the dot diameter is also large. Transport phenomena through the quantum dot can then be described in terms of the so-called Coulomb-blockade model [23]. For discussions of the success of this model and various extensions of it, we refer to [23] and [24]. We note that in this large-N regime the quantum dot is sometimes called a 'Coulomb island' [16].

So far relatively few groups claim to have probed the quantum dot energy spectrum in the few-electron regime ($N < 10$); we will discuss three examples to illustrate the various types of experimental technique available. Ashoori *et al* [25] mapped out the magnetic-field dependence of the ground-state energies $E(N)$ of an isolated, N-electron GaAs quantum dot using single-electron capacitance. This technique exploits the feature that single electrons can tunnel back and forth between an electrode and a quantum dot (through a tunnel barrier) when the chemical potential of the electrode becomes equal to the chemical potential of the dot; the chemical potential of the N-electron dot is equal to the energy required to add an extra electron to the dot, i.e. $E(N+1)-E(N)$. The resulting charge induced on the opposite electrode by this movement is then measured using a sensitive transistor. This technique hence indirectly measures ground state energies $E(N)$. A schematic diagram of their sample (taken from [25]) is shown in figure 1 together with the sample capacitance as a function of both magnetic field and gate bias for $N < 10$ (the gate-bias scale is converted to a vertical energy scale by division by a lever arm [25]). For $N > 10$ Ashoori *et al* found that a 'constant-interaction' model could explain much of the data; this model is similar to the Coulomb-blockade model discussed above in that the electron–electron interaction is treated as an additive constant to the single-electron energy, i.e. confinement and interaction effects are not treated on the same footing. However for $N < 10$ they found several deviations from this model. In particular they pointed out a bump (see figure 1) which did not appear for $N = 1$, but which was present for $N \geqslant 2$ producing a ripple-like effect with increasing N. This feature will be further discussed in section 3.1.

Meurer *et al* [26] used far-infrared spectroscopy to probe the few-electron quantum-dot energy spectrum. Their GaAs quantum dots were prepared by evaporating a gate electrode onto a photoresist structure which had been formed on top of a GaAs/GaAlAs heterostructure. Altering the gate voltage changed the number of electrons on the dot. Their measured resonance frequencies depend only weakly on the electron number (i.e. gate voltage) which seems at first sight to contradict the idea that few-electron dots have strongly N-dependent energy spectra. As will be discussed in section 3, however, this simply implies that the quantum-dot confining potential is almost parabolic since the incident radiation then only excites centre-of-mass modes [26]. They integrated the absorption strength of their spectral lines to obtain the number of electrons present in the dot as a function of gate voltage. They concluded that they were seeing discrete charging of a quantum dot with one, two, three and four electrons.

Su *et al* [27] measured resonant tunnelling through a few-electron quantum dot formed by additional lateral confinement in a double-barrier heterostructure. Their sample was constructed so that one barrier, through which electrons tunnel either onto or from the dot, was thicker (i.e. less transparent) than the other. This allowed a partial separation of the effects of confinement and charging (the charging energy includes the electron–electron

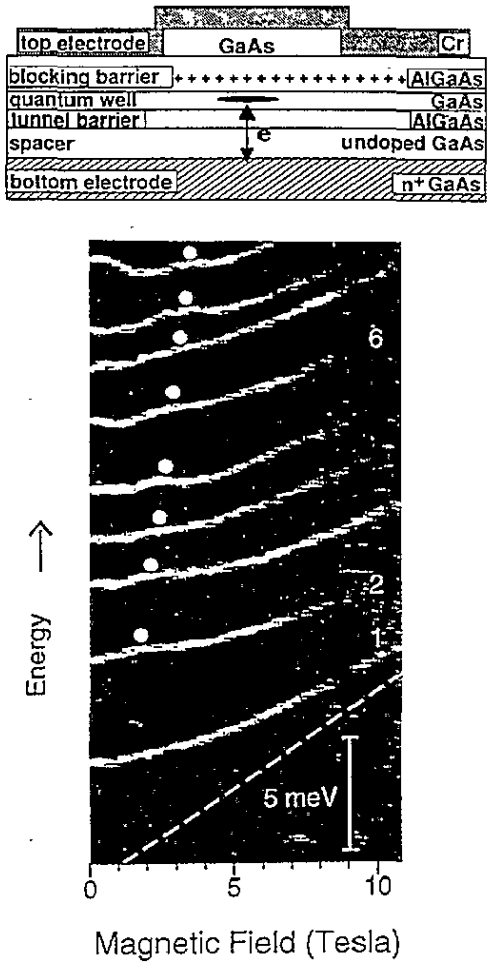

Figure 1. Experimental capacitance data of Ashoori *et al* [25] as a function of magnetic field and gate bias (energy). The white and black regions correspond to high and low capacitance respectively; the white lines provide an indirect measurement of the N-electron ground state energies [25]. Dashed line shows $\hbar\omega_c/2$. Numbers indicate number of electrons N on dot. Solid circles indicate bump which appears for $N \geqslant 2$. Schematic diagram of sample also shown. (Figure adapted from [25].)

interaction on the dot). Under 'positive-bias' conditions (i.e. with the emitter barrier for tunnelling onto the dot less transparent than the collector barrier for tunnelling off of the dot) the current reflects resonant tunnelling of just one electron at a time through the dot. The current peaks can yield information on the energy levels associated with single-electron confinement. Under 'negative-bias' conditions (i.e. with the emitter barrier more transparent than the collector barrier) electrons accumulate in the dot leading to sharp steps in the tunnelling current associated with the energy required to put an extra electron on the dot. Su *et al* concluded that the energy required for adding one more electron onto an N-electron dot was fairly insensitive to N provided $N \geqslant 3$. More recently, Tewordt *et al* [28] investigated single-electron tunnelling through ultrasmall double-barrier heterostructures with additional lateral confinement resulting from either the surface depletion potential, potential fluctuations

or single impurities.

Quantum-dot samples are often labelled as 'artificial atoms' [7]. Such a description makes sense in that the quantum dot contains a fixed number of interacting charged particles in a confined spatial region; for example, a dot containing $N = 2$ electrons is referred to as quantum-dot helium [4]. It is worth bearing in mind however that, in complete contrast with an N-electron atom such as helium, no two samples of an N-electron quantum dot fabricated from a semiconductor heterostructure can ever have exactly the same confining potential. Strictly speaking, therefore, no experimental result obtained from a given quantum-dot 'atom' can therefore be exactly reproduced in a different sample of the same 'atom'. This inherent sample dependence in atomic (dot) properties further motivates our approach in this review of highlighting *trends* in quantum-dot behaviour via analytically solvable models.

3. Theoretical background

This section discusses the various reported approaches for calculating the N-electron energy spectrum in a d-dimensional quantum dot. As discussed above, we will only consider theories of the microscopic, quantum-mechanical N-electron system which treat the electron–electron interaction on a similar quantum-mechanical footing to the kinetic energy of confinement. We will not therefore discuss semiclassical hydrodynamical models based on phenomenological Hamiltonians for large N, nor will we further consider Coulomb-blockade or constant-electron–electron-interaction models.

The few-electron quantum dot represents an interesting challenge to theorists since it marks a departure from the typical many-electron systems studied in low-dimensional semiconductor physics in the past few decades. Systems such as quantum wells and wires are strictly not nanostructures since they still have at least one free direction; the energy spectrum therefore comprises bands of allowed energies as in a bulk semiconductor. Such structures can in principle contain an infinite number of electrons and it only makes sense to talk about an electron density. Many-body effects can hence be calculated with some confidence using traditional mean-field (i.e. large-N) theories which have been used successfully in bulk semiconductors. Corrections due to electron–electron correlations can be expressed as a perturbative series in powers of $1/N$. Such approaches are likely to be suspect for quantum dots when N is small. It might appear that the correct description of a quantum dot could alternatively be imported from the formalism of atomic physics. However this may also be problematic. The two competing energy scales are the kinetic energy of the particles (which scales as the inverse square of the confinement length) and the electron–electron interaction energy (which scales as the inverse of the electron separation for a Coulomb interaction). In systems such as atoms where the confinement-length scale is small, the kinetic energy tends to dominate. Perturbative treatments of the electron–electron energy starting from a shell model are therefore reasonable and have had much success for atoms. Such a simplification for the mesoscopic regime of quantum dots is not generally possible since the kinetic energy and potential energy are typically comparable [29], both being of the order of a few millielectronvolts. A further complication is that even moderate magnetic and electric fields will introduce perturbations of this order and hence should be treated on an equal footing. In general, quantum dots represent interacting, few-body systems with a response to external fields which may lie beyond linear-response theory.

The governing equation for the energy spectrum of an isolated quantum dot is the N-particle non-relativistic Schrödinger equation. In principle this should include one-body terms such as the underlying periodic crystal potential and two-body electron–electron

interactions. However most experimental work has been carried out on quantum dots built from wide-band-gap semiconductors where the electron energies are small compared to the band gap, hence non-parabolicity effects (i.e. energy-dependent conduction-band effective mass and band-edge mixing) can be neglected. To our knowledge, all theoretical work aimed at calculating N-electron energies makes the effective-mass approximation for the electrons; generalization to few-electron dots made from HgCdTe, for example, is an open problem. Within the effective-mass approximation, the exact Schrödinger equation for N particles in a d-dimensional quantum dot having confining potential $V_C(r)$ and an external magnetic field B along the z-axis, is given by $H\Psi = E\Psi$ with $H = H_{space} + H_{spin}$; H_{space} and H_{spin} depend only on spatial and spin coordinates respectively [30]. Explicitly,

$$H_{space} = \sum_i \left[\frac{1}{2m^*} \left(p_i + \frac{eA_i}{c} \right)^2 + V_C(r_i) \right] + \sum_{i<j} V_I(r_i - r_j) \tag{1}$$

and

$$H_{spin} = g^* \mu_B B \sum_i s_{i,z} \tag{2}$$

where the momentum and vector potential associated with the ith particle are given by p_i and A_i respectively, and μ_B is the Bohr magneton. The particles have g-factor g^*, spatial coordinates $\{r_i\}$ and spin components $\{s_{i,z}\}$ along the z-axis. The eigenstates of H can be written in terms of products of spatial and spin eigenstates obtained from H_{space} and H_{spin} respectively. The z-component of total spin S_Z is equal to $\sum_i s_{i,z}$ and represents a good quantum number for the system. We have assumed the electron–electron interaction to be translationally invariant. This is not *a priori* true due to the presence of image charges in the surrounding dielectric materials and gates. However all theoretical work to date has ignored this complication.

Before turning to treatments of the exact Schrödinger equation, it is worth commenting on possible forms for the one-body confinement $V_C(r_i)$ and two-body interaction $V_I(r_i - r_j)$. Given the wide variety of confining potentials which could be used as input to a model calculation and the inherent difficulties in solving an N-body problem, it would be extremely difficult to explore the wide range of possible energy spectra for comparison with experimental data. Fortunately there is a result which gives direct information about the approximate form of $V_C(r_i)$. Kohn's theorem [31] states that the cyclotron frequency in a translationally invariant electron system is independent of the electron density and of the form of the electron–electron interaction $V_I(r_i - r_j)$. The theorem follows from the fact that the electric dipole of the radiation only couples to the centre of mass of the electrons, leaving the relative motion unchanged. This result has been generalized to parabolic quantum wells [32] and quantum dots where the confinement is parabolic [33–36]. As mentioned earlier, recent far-infrared optical measurements on artificially fabricated semiconductor quantum dots have indeed found the absorption frequencies to be essentially independent of the number of electrons [4]; this implies that the bare confining potential is nearly parabolic. Such a parabolic confinement is consistent with simple electrostatic considerations. The two-body electron–electron interaction $V_I(r_i - r_j)$ between electrons i and j would of course vary as $|r_i - r_j|^{-1}$ in free space. However in quantum-dot structures, the form of $V_I(r_i - r_j)$ may be modified in a non-trivial way by the presence of image charges in adjacent layers and gates. Furthermore, the wavefunctions of electrons in two- (and one-) dimensional quantum dots have a small but finite extent in the remaining strongly confined directions. This results in a slight smearing of the electron charge, modifying the pure Coulomb form appropriate to point charges.

3.1. Exact numerical calculations

One approach is to try solving the N-particle Schrödinger equation $H\Psi = E\Psi$ numerically. A basis set made up from products of single-particle states is employed, the matrix elements of H calculated and the resulting matrix diagonalized [33, 37]. Given a powerful enough computer, this approach can in principle yield the exact result. The decision of how to truncate the resulting matrix (i.e. choosing a finite basis set) is crucial. The calculations are computationally intensive since the size of the matrix required for good accuracy increases rapidly with N; such calculations must trade off increasing electron number N with a reduced number of single-particle basis states. Since the resulting eigenvalues can be closely spaced in energy, the overall ground state may become difficult to predict for large N given the uncertainties introduced by the numerical procedure. One of the first few-electron studies was by Laughlin for $N = 3$ electrons in a $d = 2$ parabolic potential in the presence of a magnetic field [38]. Laughlin was specifically interested in understanding the origin of the novel ground states giving rise to the FQHE in a two-dimensional electron gas. Since the FQHE had been observed at relatively large magnetic field, only single-particle states in the lowest spin-polarized Landau level were included in the basis. The calculations showed that the ground-state angular momentum J of the three electrons increased with magnetic field and followed a 'magic-number' sequence $J = 3m$ where m is an integer. Girvin and Jach then carried out a numerical diagonalization for $N = 3, 4$ and 5 electrons in $d = 2$ dimensions [39]. Again since the motivation was the explanation of the FQHE, the single-particle basis states were limited to the lowest spin-polarized Landau level. They found that the 'magic-number' angular momenta for N electrons were separated by N units of angular momentum, a direct generalization of the $N = 3$ result mentioned above. Girvin and Jach [39] raised the point that these angular momenta J for $N = 3$, when converted to an effective filling factor using $\nu = N(N-1)/2J$, yielded the sequence $\nu = 1, \frac{1}{2}, \frac{1}{3}$, etc. and that unfortunately $\nu = 1/2$ had not been observed in FQHE measurements on the 2DEG. Maksym and Chakraborty [33] presented a calculation for a $d = 2$ parabolic dot with $N = 3, 4$ spin-polarized electrons. They found ground-state angular momenta which followed the same sequence with increasing magnetic field and pointed out that these transitions in the ground state should show up in low-temperature magnetization measurements. By looking at the charge density distribution, such few-particle calculations show the emergence of what have been termed Wigner molecules which are finite-N precursors of Wigner crystals [40, 41]. Maksym and Chakraborty subsequently generalized their calculations to account for non-spin-polarized electrons [42]. At low magnetic field the jumps in the ground-state angular momenta are accompanied by jumps in the total spin. Such behaviour is a direct consequence of the requirement that the total N-electron wavefunction be antisymmetric. A simplified version of this behaviour was also reported for quantum-dot helium (i.e. $N = 2$, $d = 2$); in this case the jumps in total spin can be labelled simply as 'spin-singlet–spin-triplet' transitions [43]. Angular-momentum jumps in quantum-dot helium are further discussed in section 4.2.

Hawrylak and Pfannkuche reported similar ground-state transitions for small N [44] and Hawrylak subsequently proposed [45] an identification with various features seen in the data of Ashoori *et al* [25] discussed in section 2. Figure 2 (taken from [45]) compares the measured [25] and calculated energies for adding a third electron to an $N = 2$ quantum dot as a function of magnetic field. MacDonald and co-workers have reported a rich phase diagram of magic-number ground states for $N = 5, 6$ electrons in a $d = 2$ parabolic potential [46]. They used their calculations to propose the possibility of mesoscopic oscillations in the thermodynamic properties of an N-electron dot with a period which is a multiple of the period for free electrons [47]. All of these numerical calculations take the form of

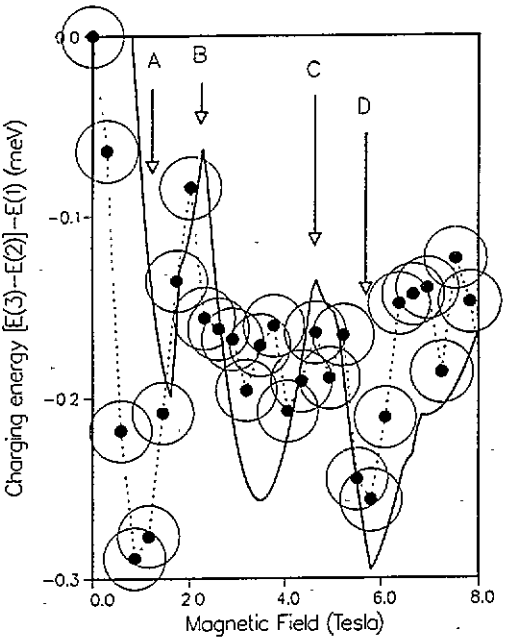

Figure 2. Numerical calculation of Hawrylak (solid line [45]) for energy to add a third electron to an $N = 2$ electron dot (labelled 'charging energy') compared to the measured values of Ashoori *et al* (solid circles [25]—dotted line is a guide). The energy has $E(N = 1)$ subtracted ($\{E(3) - E(2)\} - E(1)$). Size of circle shows experimental error. Letters A, B, C and D correspond to spin and angular-momentum ground-state transitions in the $N = 2$ and $N = 3$ electron dot [45]. D is mostly due to the angular-momentum ground-state transition $1 \rightarrow 3$ in the $N = 2$ electron dot which is further discussed in section 4.2. (Figure taken from [45].)

the electron–electron interaction to be the bare Coulomb form. Kinaret *et al* have shown numerically that quantitatively similar results follow if one assumes the electron–electron interaction to be of inverse-square form [48]. This form of the electron–electron interaction is discussed further in section 4.

There have been numerical calculations in other geometries. The first was by Bryant [49] for $N = 2$ electrons in a $d = 2$ rectangular box with infinite-potential walls and zero magnetic field. Bryant investigated the interplay of the kinetic energy ($\sim L^{-2}$) and the potential energy ($\sim L^{-1}$) as a function of the size of the box L_x, L_y. He found the energy spectrum to depend strongly on the aspect ratio L_x/L_y. For sufficiently large L the potential energy dominates and the possible precursor of a Wigner solid can be seen in both 1D ($L_x \gg L_y$) and 2D ($L_x \sim L_y$) limits (the ground state becomes degenerate). In section 4.1, we show the extent to which Bryant's numerical results can be understood using analytically solvable models. Kramer and co-workers [50] have carried out a numerical calculation for $N = 3$ and 4 electrons in a rectangular box $L_x \gg L_y$ (i.e. $d = 1$) using a 'pocket-state' basis approach. This approach exploits the potential-energy minima associated with the classical N-electron configurations to introduce a finite set of approximate, localized basis functions for the N-electron system in configuration space; the Hamiltonian is then diagonalized within this basis [50]. Similar results are seen as for $N = 2$. For small L_x the single-particle confinement energy dominates; the charge density of the ground state is essentially homogenous. As L_x increases the potential energy begins to dominate and

the electrons form an inhomogenous charge distribution resembling a blurred version of the classical limit of equispaced point charges (Wigner molecule). Chui [51] also carried out a diagonalization for few electrons in a quasi-1D electron system. He found an energy gap at half-integer filling which may be related to the FQHE fraction near half filling observed experimentally in one-dimensional ballistic constrictions [52].

3.2. Many-body perturbation theory

For $N > 6$ it becomes exceedingly difficult to perform a direct numerical diagonalization; for sufficiently large N, standard many-body techniques should prove useful for obtaining information about trends with increasing N. One of the first many-body perturbation calculations in a quantum dot was carried out by by Kumar *et al* [53] who employed the Hartree approximation for a realistic quantum-dot geometry. More recently Hartree calculations have been carried out for up to 30 electrons [54]. The accuracy of the Hartree and Hartree–Fock approximation for few-electron quantum dots has been investigated [55, 56]. It was found for $N = 2$ [55] that the Hartree approximation was inaccurate due to the unphysical self-energy corresponding to each electron interacting with itself. In the Hartree–Fock approximation this self-energy is cancelled by the exchange interaction; however, the results of Pfannkuche *et al* [55] show that for small N, even the Hartree–Fock approximation can not be relied upon for accurate results due to neglect of correlation effects (i.e. its accuracy for a given magnetic field depends on the particular $N = 2$-electron ground state in question [55]). We will not continue discussion of many-body perturbation methods since we are explicitly interested in the small-N regime where the exact numerical diagonalizations of section 3.1 are more accurate.

3.3. Analytically solvable models

There have been two alternative approaches at investigating general features of few-electron quantum-dot energy spectra without resorting to detailed numerical calculations. The first involves the use of analytically solvable microscopic models for the N-electron interacting system. The resulting energy expressions directly display trends in the N-electron energy spectrum as a function of the dot parameters. The second, to be discussed in section 3.4, is a more abstract group-theoretical approach. Obviously the general N-electron Hamiltonian H cannot be solved exactly analytically. However using model confinement potentials and model electron–electron interactions, exact analytical results can indeed be obtained for $N \geqslant 2$. All such models to date exploit the fact that the approximate confinement potential in the actual samples seems to be well approximated by a parabolic potential as discussed earlier. In section 4 it will be shown that such analytically solvable models can often capture the basic physics emerging from the numerical calculations for few electrons.

Taut [57] managed to obtain exact analytic results for $N = 2$ electrons interacting via a Coulomb interaction in $d = 2$ dimensions for *specific* values of the magnetic field and parabolic confining potential. Generalization to arbitrary magnetic field and/or $N > 2$ with the Coulomb interaction is an open problem. As mentioned above Kinaret *et al* [48] have shown numerically that an inverse-square form of the electron–electron interaction αr^{-2} gives very similar results to the bare Coulomb form βr^{-1} in $d = 2$ dimensions. This inverse-square interaction resembles the dipole-like form used in [16] to allow for image charge effects. In [58] it was shown that the energy spectrum of $N = 2$ electrons interacting with the inverse-square interaction αr^{-2} in $d = 2$ dimensions is exactly solvable for arbitrary values of the magnetic field. The exact solution includes mixing with all Landau levels. The singlet–triplet transitions found for the Coulomb interaction [43] are reproduced

exactly using the inverse-square interaction. This result was subsequently extended to obtain approximate analytic results for $N > 2$ ($d = 2$) [59]. For $d = 1$ dimension and zero magnetic field, the N-electron model with inverse-square interactions was solved by Calogero for any N [60]. This result has recently been used [61] to explain the periodic conductance oscillations observed experimentally in narrow 1D quantum dots [7].

The only exactly solvable model known to us for $N > 2$ electrons in $d > 1$ dimensions with a magnetic field is that of the harmonic interaction studied in [39] with a restriction to lowest-Landau-level basis states, and then subsequently solved exactly (i.e. including mixing with all Landau levels) [62]. This model [62] was subsequently used to calculate exciton energies in a quantum dot [63], to investigate the high-magnetic-field excitation spectrum of a quantum dot [64], to discuss Coulomb- and Pauli-blockade effects during resonant tunnelling through a quantum dot [65] and to predict dimensional instabilities in a three-dimensional anisotropic dot [66].

3.4. Group theory

The above-mentioned exact results for an $N = 2$ electron pair could in principle be used in a coupling procedure to tackle the N-electron problem. Such an approach already exists in nuclear physics via group theory. More generally, group-theoretic techniques borrowed from nuclear physics should prove useful in unravelling the energy spectrum of an quantum dot because of the analogy with N strongly interacting nucleons in a d-dimensional nucleus. In particular a parabolic (i.e. harmonic-oscillator) confining potential is often employed in nuclear physics. The properties of symmetry groups related to the harmonic oscillator have therefore been studied extensively [67]. The requirement that the total N-electron wavefunction be antisymmetric under the interchange of any two electrons places an additional symmetry restriction on the eigenstates of H; not all the mathematically allowed solutions of $H\Psi = E\Psi$ are necessarily physically allowed. Since there are only two possible values of the single electron spin, the symmetry of the spin configuration (i.e. the so-called spin partition) places a strong restriction on the allowed spatial configurations (spatial partitions). Given the range of possible N values in a given quantum-dot experiment, it would be a significant advance if some 'fingerprints' could therefore be obtained whereby one would know that the occurrence of a given multiplet of conduction peaks in the experimental data signalled that the quantum dot contained $4 \leqslant N \leqslant 6$ electrons, as opposed to $8 \leqslant N \leqslant 10$. The physical symmetries and state classification of an N-electron gas in a d-dimensional quantum dot were studied in [68] using the symplectic group framework. [69] took this approach one stage further by calculating analytically the energies of a class of N-electron algebraic Hamiltonians built from the symplectic group chain. Non-parabolicity and particle–particle interactions were simulated using quadratic Casimir operators. Previous calculations for non-parabolic quantum dots containing N interacting electrons [54, 70] considered realistic microscopic perturbations to the N-electron Hamiltonian, and calculated numerically the shifts of the energy levels using perturbation theory. The Casimir operator approach provides *approximate* descriptions of actual perturbations and then gives the energy shifts *exactly*. Such an approach, while not common in condensed-matter physics, is well known in nuclear and molecular physics for describing rotational and vibrational band structures.

4. Energy spectrum of a few-electron quantum dot

We now explore the extent to which the energy spectrum of a few-electron quantum dot can be understood using analytically solvable models, with a view to obtaining trends in

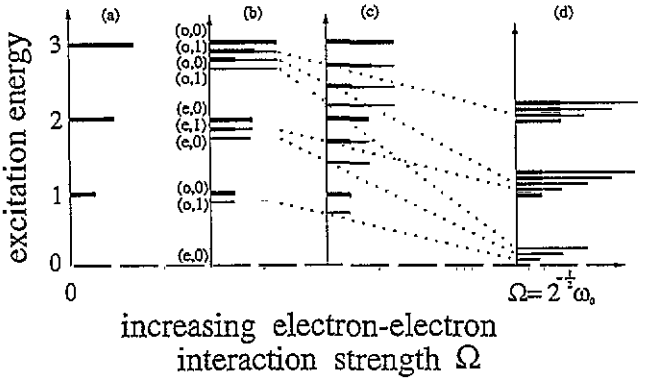

Figure 3. Analytical energy-level spectrum for $N = 2$ electrons in a $d = 1$-dimensional parabolic quantum dot for increasing values of the harmonic electron–electron interaction strength Ω ((a)–(d)). Energies are shown in units of $\hbar\omega_0$ with respect to the ground state. For each excitation energy level, the lengths of the thick (thin) lines represent the number of quanta of centre-of-mass- (relative-) mode excitation. The labellings in parentheses (P, S) denote the parity P (e = even, o = odd) and total spin S of each level for the purpose of comparison with Bryant's Coulomb calculation [49]. In (a), $\Omega = 0$ while in (d), $\Omega = 2^{-1/2}\omega_0$ (i.e. $\Omega_0 = 0$). Spectra (a)–(c) are qualitatively the same as for Bryant's numerical diagonalization calculations (figure 1 of [49]).

electronic properties. We will tend to focus on quantum-dot helium ($N = 2$) since it is the simplest example of a dot containing interacting electrons [4]. The confining potential for the analytically solvable models is taken to be parabolic ($\hbar\omega_0$), hence the total energy can be written as $E = E_{CM} + E_{rel} + E_{spin}$ where E_{CM} is the centre-of-mass energy, E_{rel} is the relative-mode energy and E_{spin} is the spin energy. The translationally invariant electron–electron interaction $V_I(r)$ (r is the electron–electron separation) only affects the spectrum of E_{rel} and hence the relative-coordinate wavefunction. The numerical results mentioned below employ the Coulomb interaction $V_I(r) = \beta r^{-1}$. The analytically solvable models in d dimensions are $V_I(r) = \alpha r^{-2}$ (inverse-square interaction) and $V_I(r) = dV_0 - \frac{1}{2}m^*\Omega^2 r^2$ (harmonic interaction) where α, V_0 and Ω are positive parameters.

4.1. 1D quantum dot

Most studies of a one-dimensional quantum dot (1DQD) consider zero external magnetic field, hence $E_{spin} = 0$. For one electron in a parabolic dot, the energy spectrum is trivially

$$E = E_{CM} = \hbar\omega_0(K + \tfrac{1}{2}) \tag{3}$$

where K is a positive integer or zero. This expression for the centre-of-mass spectrum E_{CM} is valid for arbitrary N. For $N = 2$ electrons the exact relative energy E_{rel} for the inverse-square interaction is given by

$$E_{rel} = \hbar\omega_0(2k + s + \tfrac{1}{2}) \tag{4}$$

where $s = (\tau + \frac{1}{2})$ with $\tau = \frac{1}{2}(1 + 4m^*\alpha/\hbar^2)^{1/2}$; k is a positive integer or zero. The exact relative energy for the harmonic interaction is given by

$$E_{rel} = V_0 + \hbar\Omega_0(k + \tfrac{1}{2}) \tag{5}$$

where $\Omega_0^2 = \omega_0^2 - 2\Omega^2$. Energies for $N = 2$ electrons in a 1DQD with Coulomb interaction were calculated numerically in [49].

Figure 3 shows the analytically obtained excitation spectrum for an $N = 2$ 1DQD with harmonic electron–electron interaction for increasing values of the interaction strength Ω. In figure 3(a) $\Omega = 0$ while in figure 3(d) $\Omega = 2^{-1/2}\omega_0$ (i.e. $\Omega_0 = 0$). The excitation energy for a given K and k is shown as a line with a length proportional to $K + k$. The centre-of-mass contribution is shown as a thick section of length K while the relative-mode contribution is a thin section of length k. For odd (even) k, the spatial part of the wavefunction is antisymmetric (symmetric) and hence the spin part of the wavefunction must be symmetric (antisymmetric). The corresponding value of the spin $S = 1$ ($S = 0$) is also indicated in figure 3. The triplet ($S = 1$) levels are triply degenerate. The sequence of spectra shown in figure 3(a)–(d) is qualitatively the same if Ω is held constant while ω_0 is reduced from $\omega_0 \gg \Omega$ (i.e. strong confinement) to $\omega_0 = 2^{1/2}\Omega$. The sequences of energy levels shown in figure 3(a)–(c) are qualitatively the same as for Bryant's exact numerical calculations (see figure 1 of [49]). Increasing the box length L in Bryant's calculation corresponds to reducing ω_0 since the characteristic oscillator length (i.e. effective box length) varies as $\omega_0^{-1/2}$. This correspondence is remarkable since Bryant's calculation was for two electrons confined in a narrow box with infinite potential walls as opposed to a harmonic confinement, and interacting via a Coulomb interaction as opposed to a harmonic interaction. The energy-level sequence therefore appears relatively insensitive to details of the one-body confinement or the two-body interaction. For large electron–electron interaction or small ω_0 (i.e. large dot size), the harmonic interaction spectrum deviates from the Coulomb result; the electron–electron interaction no longer represents a small perturbation and hence its particular analytic form becomes important. In figure 3, all the relative-mode energy levels become degenerate as ω_0 approaches $2^{1/2}\Omega$ (figure 3(d)). In the Coulomb spectrum of [49] only the lowest two levels are shown as becoming degenerate for large L. The degeneracies in both models suggest an instability of the system and a possible precursor to Wigner-solid formation [49].

For $N = 2$ electrons interacting via the inverse-square interaction αr^{-2}, the situation is different in that any non-zero α immediately yields degeneracy of the lowest two levels with $S = 0$ and $S = 1$. In [49] (and in figure 3(d)) this degeneracy was only reached in the large-L limit where the electron–electron interaction dominated the kinetic energy. The inverse-square interaction is singular and hence always behaves as a large perturbation to the system; it does not allow interchange of the two electrons for any finite α (the tunnelling barrier for interchange becomes inpenetrable). In the centre-of-mass frame the electron density falls exactly to zero as the two electrons approach each other; the system therefore has the character of a true Wigner solid and not just a charge-density wave. The relative mode energy spectrum has level spacing $2\hbar\omega_0$ for all values of α (see equation (4)).

For $N > 2$ electrons in a rectangular box, the numerical results of Kramer *et al* with a cut-off Coulomb interaction show a similar tendency to that of [49] for Wigner crystallization at sufficiently large box length [50]. The energy spectrum for $N > 2$ with a harmonic interaction is qualitatively similar to figure 3; the number of levels in a given multiplet will increase with N and the relative-mode energy spacing is now $\hbar\Omega_0 = \hbar(\omega_0^2 - N\Omega^2)^{1/2}$. The instability within the harmonic-interaction model now occurs at a larger ω_0 value (i.e. shorter box) given by $N^{1/2}\Omega$. The inverse-square model for $N > 2$, as for $N = 2$, is unstable to formation of an ordered electron chain and electron–electron interchange is forbidden for any non-zero α. This model was first solved exactly by Calogero [60]. The exact N-electron energy levels are given by $E(N; K, k) = E_{CM}(K) + E_{rel}(N; k)$ with

$$E_{rel}(N; k) = \hbar\omega_0\left(\tfrac{1}{2}(N-1) + \tfrac{1}{2}N(N-1)(\tau + \tfrac{1}{2}) + k\right). \tag{6}$$

Note that $k = 1$ is not allowed. Although the Calogero model is strictly one dimensional, it still manages to explain qualitative features of the conductance peaks in measurements

of transport through narrow quantum dots whose lateral dimensions are small but non-zero [7]. Given that the quantum dot is weakly coupled to the reservoirs, the conductance-peak positions will directly depend on the N-electron spectrum of the isolated dot $E(N; K, k)$; conductance peaks are expected when the kinetic energy of the incoming $(N+1)$ electron is equal to $E(N+1; K', k') - E(N; K, k)$. For small tunnelling voltage bias applied along the length of the channel, the ground-state tunnelling process dominates (i.e. $K = K'$, $k = k'$) and the exact spacing between conductance peaks calculated within the model is given by [61] $\delta = \hbar\omega_0(\tau + \frac{1}{2})$; this N-independent form is consistent with the experimental findings [7]. The experimentally observed periodic conductance peaks have motivated the proposal of a single-electron transistor [7]. For strong electron–electron interaction, the peak spacing $\delta \to (m^*\alpha)^{1/2}\omega_0$ and is independent of $\hbar$, thereby making contact with classical Coulomb-blockade charging models. For larger tunnelling-voltage biases, excited-state tunnelling processes are possible ($k \neq k'$ and/or $K \neq K'$) yielding a much smaller additional conductance-peak spacing $\delta = \hbar\omega_0$ which is again consistent with experiment (see figure 4 of [7]).

There are a number of other exactly analytically solvable 1D models based on inverse-square interactions which are often referred to as Sutherland models [71]. These differ from the Calogero model in that they have periodic boundary conditions and hence give fundamentally different N-electron energy spectra. In contrast to the Calogero model, they cannot reproduce the experimental observation of periodic conductance oscillations. Sutherland models prohibit edge states by imposing periodic boundary conditions; the Calogero model with its parabolic confining potential has the N-electron wavefunction and its derivative vanishing at infinity and every state becomes an edge state. Periodic boundary conditions are equivalent to taking the form of the inverse-square electron–electron interaction as $(\sin(\pi(x_i - x_j)/L))^{-2}$, this being the interaction for two electrons on a ring of radius $L/2\pi$ with x measured along the circumference. Such models are inappropriate for 1D quantum dots weakly coupled to source and drain reservoirs; however they may prove useful for investigating electron–electron interaction effects in quantum rings (so-called quantum 'doughnuts'). Although the two types of model describe different physical situations, there are subtle connections between the two via the field of quantum chaology. In particular it has recently been shown [72] that the dynamical correlations in these quantum-mechanical models are related to spectral correlations in quantum chaotic systems.

There has been a recent proposal of a crystal-like excitonic phase as the ground state of a 1D system of singlet excitons (i.e. electron spin up and hole spin down) [73]. It would be interesting to investigate the analogy in a 1DQD within the analytically solvable models discussed here. The solution for one electron and one hole with an inverse-square interaction (attraction) can be obtained from (4) by setting $\alpha \to -\alpha$, and introducing a reduced mass μ. There is now a critical value of the electron–hole interaction parameter $\alpha_0 = \hbar^2/8\mu$. For $\alpha > \alpha_0$ the electron–hole pair (i.e. the exciton) cannot be formed, while for $0 < \alpha < \alpha_0$ the electron–hole pair can become stable.

4.2. 2D quantum dot

The energy spectrum for $N = 1$ electron in a $d = 2$-dimensional parabolic potential with a perpendicular magnetic field has been extensively discussed in the literature [6, 74]. The single-particle Schrödinger equation is easily solved in the symmetric gauge giving energy solutions $E = E_{\text{space}}(n, m) + E_{\text{spin}}$ where

$$E_{\text{space}} = E_{\text{CM}} = \hbar\omega_0(B)(2n + |m| + 1) - \tfrac{1}{2}m\hbar\omega_c \tag{7}$$

where $\omega_0^2(B) = \omega_0^2 + \omega_c^2/4$ and n is a positive integer or zero. The angular momentum m can be any integer or zero.

Consider the case of $N = 2$ electrons. The total energy $E = E_{CM}(n', m') + E_{rel}(n, m) + E_{spin}$. The exact relative energies $E_{rel}(n, m)$ for the inverse-square interaction are given by

$$E_{rel} = \hbar\omega_0(B)(2n + s + 1) - \tfrac{1}{2}m\hbar\omega_c \tag{8}$$

where the relative angular momentum m is any integer or zero, n is any positive integer or zero and $s = (m^2 + m^*\alpha/\hbar^2)^{1/2}$. For the parabolic interaction

$$E_{rel} = 2V_0 + \hbar\Omega_0(B)(2n + |m| + 1) - \tfrac{1}{2}m\hbar\omega_c \tag{9}$$

where $\Omega_0^2(B) = \omega_0^2 + \omega_c^2/4 - 2\Omega^2$.

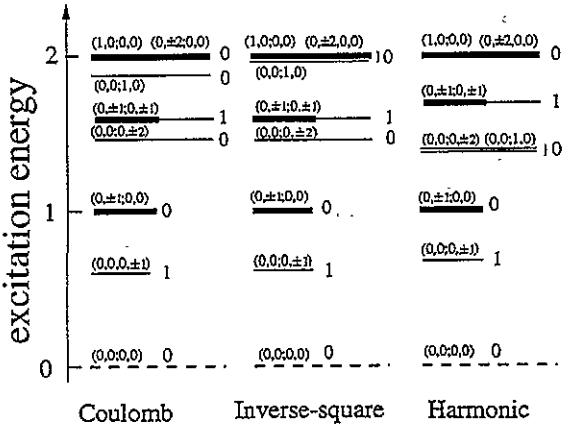

Figure 4. Theoretical energy-level spectrum for $N = 2$ electrons in a $d = 2$ dimensional parabolic quantum dot at zero magnetic field for various forms of the electron–electron interaction. Energies are shown in units of $\hbar\omega_0$ with respect to the ground state. Expressions for the harmonic and inverse-square interaction levels are obtained analytically. The Coulomb spectrum is adapted from the numerical results of [75]. Lengths of thick and thin lines represent the number of centre-of-mass and relative quanta respectively, as for figure 3. Total spin S is indicated to the right of each level. Labellings in parentheses $(n', m'; n, m)$ denote centre-of-mass- and relative-mode quantum numbers for the purpose of comparison with the Coulomb result.

We first discuss zero magnetic field for $N = 2$. The sequence of excitation energies for the three forms of the electron–electron interaction of interest is shown in figure 4. The sequence of excitation energies for the Coulomb interaction is taken from the numerically obtained results of [75]. Analytic expressions for the energies with the inverse-square and harmonic interactions are easily obtained from $E = E_{CM} + E_{rel}$. For each excitation-energy level, the lengths of the thick and thin portions denote the number of quanta of centre-of-mass- and relative-mode excitation respectively. The corresponding quantum numbers are indicated in parentheses $(n', m'; n, m)$; the total spin S is also indicated. The spectra for the Coulomb and inverse-square interactions are almost identical; the harmonic interaction is qualitatively similar. For both the inverse-square and harmonic interactions, there is an extra degeneracy in the higher-energy multiplet as compared with the Coulomb result. This

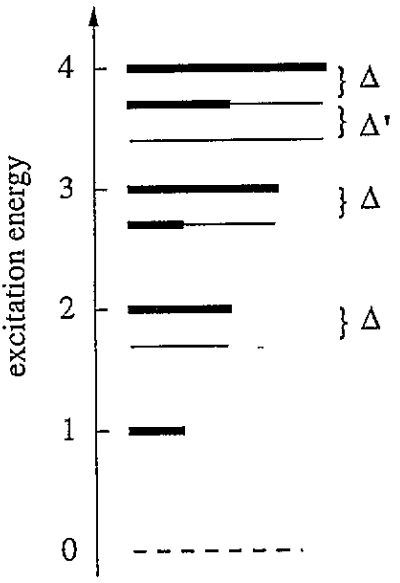

Figure 5. Schematic energy-level structure for $N = 2$ electrons in a $d = 2$ dimensional parabolic quantum dot at moderate magnetic field (i.e. $n' = 0$, $n = 0$ for low-lying energy levels; electrons are spin polarized) for harmonic and inverse-square interactions. The energy-level spacing $\Delta = \Delta'$ for the harmonic interaction, while $\Delta \neq \Delta'$ for the inverse-square interaction. Lengths of thick and thin lines represent the number of centre-of-mass and relative angular-momentum quanta m' and m respectively. Energies are indicated in units of $\hbar(\omega_0(B) - \omega_c/2)$ with respect to the ground state.

reflects extra hidden symmetries in the two-electron Hamiltonians with these interactions as compared with the Coulomb interaction, and partially explains their exact solvability.

Figure 5 shows the $N = 2$ energy spectrum for the inverse-square and harmonic interactions at moderate magnetic field such that all the low-lying energy states correspond to $n' = 0$ and $n = 0$. The g^*-factor is taken to be sufficiently large that the electrons are spin polarized. The ground state has $m' = 0$ and $m = 1$. The two forms of the interaction give qualitatively similar results; the excitation gap $\Delta = \Delta'$ for the harmonic interaction, whereas $\Delta \neq \Delta'$ for the inverse-square interaction.

As the magnetic field increases further, the low-lying energy levels all have $n' = 0$, $n = 0$, $m' = 0$ and $m > 0$. Wagner *et al* [43] showed numerically for the Coulomb interaction that the ground state undergoes transitions to progressively higher relative-angular-momentum m values ($1 \rightarrow 3 \rightarrow 5 \rightarrow \ldots$ for a spin-polarized system due to the requirement of total wavefunction antisymmetry). At such large magnetic fields (large ω_c) the single-electron (i.e. non-interacting) energy-level spacings are small ($\hbar(\omega_0(B) - \omega_c/2) \sim \hbar\omega_0^2/\omega_c$). We might therefore expect the energy-level spectrum of the interacting electron system to depend more on the specific form of the electron–electron interaction since the interaction no longer represents a small perturbation. However it was shown analytically in [58] that the inverse-square interaction yields an identical sequence of ground-state transitions to the Coulomb interaction with increasing magnetic field. Within this analytic model (i.e. equation (8)), these transitions can be understood as arising from the fact that E_{rel} has a minimum at finite $m = m_0$ where $m_0 \sim (\alpha m^*/\hbar^2)^{1/2}(\omega_c/2\omega_0)$ [58] as shown in figure 6. In contrast the harmonic interaction does not show such angular-momentum transitions of the ground state. This characteristic behaviour of the harmonic-interaction model is in

fact generic for any N and can be understood as follows. The dot of N electrons interacting with a harmonic interaction necessarily satisfies $\omega_0 > N^{1/2}\Omega$ otherwise electrons would leave the dot. The ground state has the lowest possible angular momentum J consistent with the total wavefunction antisymmetry. For spin-polarized electrons, $J = N(N-1)/2$ (the wavefunction has Vandermonde form) where $J = 1$ for $N = 2$. Consider the limit as $\omega_0 \to N^{1/2}\Omega$. The excitations of purely relative character (see thin lines in figure 5 for $N = 2$, and in [64] for $N \geqslant 2$) become degenerate with the ground state. For $\omega_0 < N^{1/2}\Omega$, these excited states with higher J are lower in energy than the original ground state, i.e. higher-J modes have become soft. In fact, the higher the J value of the state, the lower the energy. The Nth electron therefore goes into an orbit with infinite radius (infinite J) i.e. it leaves the dot. The dot now contains $N-1$ electrons such that $\omega_0 > (N-1)^{1/2}\Omega$. Figure 7 summarizes this difference in behaviour of the Coulomb and inverse-square interactions (figure 7(a)) against the harmonic interaction (figure 7(b)) for a pair of electrons. The harmonic interaction therefore only gives results which are qualitatively similar to the Coulomb and inverse-square interactions in the limit of small electron–electron interaction strength (Ω) compared to the confinement (i.e. in the limit of large ω_0 and hence small effective dot radius). This finding is consistent with that found for a 1DQD (see figure 3). We note that for an *anharmonic* electron–electron interaction, this qualitative agreement can be restored. If one considers a (cut-off) Coulombic interaction as a Taylor series in the electron–electron separation r, the harmonic-interaction model represents the exact results to order r^2. One can now treat the quartic term $-r^4$ in perturbation theory. For large electron–electron separations, the quartic term will tend to dominate and bind the Nth electron at a large but finite radius yielding a high-J ground state, consistent with the Coulomb and inverse-square models.

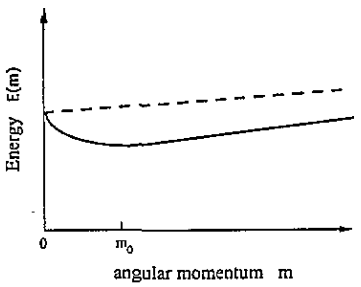

Figure 6. Analytical relative-mode energy $E(m) = E_{\rm rel}(n = 0, m)$ against relative angular momentum m (treated as continuous) for $N = 2$ electrons in a $d = 2$ parabolic dot $\hbar\omega_0$ with an inverse-square interaction (solid line) at a fixed magnetic field ω_c. The same curve for the harmonic interaction is linear (dashed line) and has positive slope if $\Omega < 2^{-1/2}\omega_0$.

For $N \geqslant 2$ electrons ($d = 2$) at low magnetic field, the energy spectra are expected to be strongly N dependent (cf. spectra of atomic He, Li etc.). Unlike the inverse-square interaction, the harmonic interaction is still exactly analytically solvable. Given the qualitative agreement with the Coulomb interaction for $N = 2$ in the case where the electron–electron interaction is not too large a perturbation to the single-electron energies, it is reasonable to expect the harmonic interaction to be a realistic model for $N \geqslant 3$ for small dots (i.e. large ω_0). A true Coulomb interaction would simply produce some small additional degeneracy splittings of the harmonic-interaction-model energy spectrum, similar to those shown in figure 4. Figure 8 shows the analytically obtained spectra for $N = 2$

(quantum-dot helium) and $N = 3$ (quantum-dot lithium) with a harmonic interaction in a small dot (large ω_0) at low magnetic field. The strong N dependence of the spectra is striking. Such characteristic multiplet structures could act as 'fingerprints' for deducing the number N of electrons in a given dot from the conductance-peak structure obtained in transport measurements. We note that the harmonic-interaction model can be used to generate energy spectra for all N, yielding a 'periodic-table' classification for quantum dots.

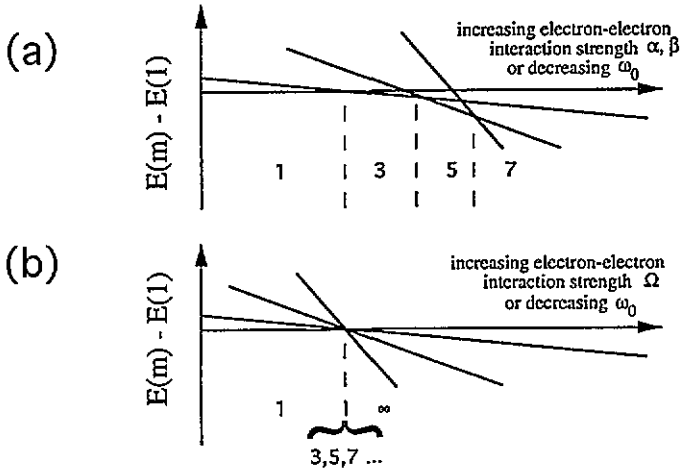

Figure 7. Schematic diagram showing the relative-mode energy $E(m)$ (measured with respect to $E(m = 1)$) for $N = 2$ spin-polarized electrons in a $d = 2$ parabolic dot as a function of increasing electron–electron interaction or decreasing dot confinement strength for (a) Coulomb and inverse-square interaction (i.e. increasing β and α or decreasing ω_0), and (b) harmonic interaction (i.e. increasing Ω or decreasing ω_0) at a given magnetic field. The ground-state m values are indicated beneath.

For $N \geqslant 3$ electrons at large magnetic fields interacting via a Coulomb interaction, direct numerical diagonalization calculations have been carried out by many groups as mentioned earlier. Transitions to ground states of increasing total angular momenta were found; such 'magic' J values are the $N \geqslant 3$ equivalent of the $N = 2$ values discussed above. As noted earlier the angular momenta of these ground states, when converted to effective filling factors, do not seem to yield a sequence which agrees with the observed FQHE values in the 2DEG [39]. The inverse-square interaction is no longer exactly solvable for $N \geqslant 3$; however it has recently been solved approximately using a simple pairing procedure [59]. Coincidentally, all the stable fractions ν predicted by the model [59] have been observed experimentally in the 2DEG. The harmonic interaction is still exactly solvable for any N at any magnetic field. Within this model, it was shown [64] at high magnetic field that the excitation energies exhibit complex crossings as a function of the strength of the electron–electron interaction. A fundamental difference was found between the $N = 2$- and $N > 2$-electron excitation spectrum; the energy spectrum in figure 5 gains some additional relative modes which are not possible for the $N = 2$ spectrum. The reason [64] is that for $N = 2$ all possible relative excitations have wavefunctions of Jastrow form while for $N \geqslant 3$ this is no longer the case. It is sometimes stated that the Laughlin wavefunction is an exact eigenstate of the N-electron problem including harmonic

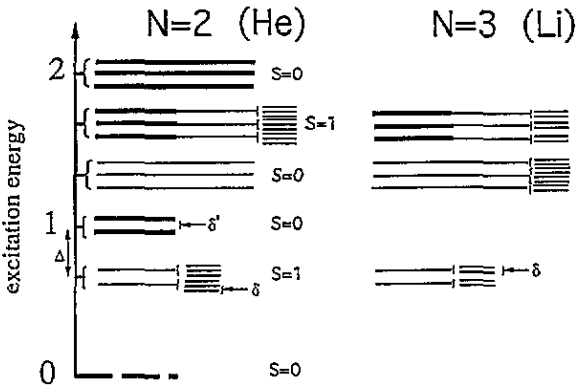

Figure 8. Analytical energy spectra for $N = 2$ and $N = 3$ electrons at low magnetic field in a $d = 2$ parabolic dot with a harmonic interaction. The spin splitting $\delta = (g^*m^*/2m_0)\hbar\omega_c$; the splitting $\delta' = \hbar\omega_c$. The spacing $\Delta = \hbar(\omega_0(B) - \Omega_0(B))$. Total spin S for $N = 2$ is indicated. Energies are shown in units of $\hbar\omega_0(B)$ with respect to $E_0 = \hbar\omega_0(B) + (N-1)\hbar\Omega_0(B) + N(N-1)V_0$; E_0 represents the ground state for $N = 2$ but is disallowed for $N = 3$ due to the Pauli principle. Lengths of thick and thin lines represent the number of centre-of-mass- and relative-mode quanta.

interactions; this is incorrect. The exact many-body wavefunctions for the excited states are *generalizations* of Laughlin wavefunctions [64]. The electron–electron interaction causes significant *inter*-Landau level mixing of the single-electron levels. As shown in figure 7(b) and discussed above, for a dot confinement potential ω_0 weaker than the critical value $N^{1/2}\Omega$, or alternatively above a critical value of the effective dot radius, the system with harmonic interactions becomes unstable to formation of ground states with arbitrarily high angular momenta. For a more realistic form of the electron–electron interaction, this instability manifests itself in the formation of fractional ground states with finite $\nu < 1$. In the language of the fractional quantum Hall effect (FQHE) the harmonic-interaction model is only realistic if the impurity potential represented by the dot ($\hbar\omega_0$) is strong enough as to break the FQHE, i.e. $\omega_0 > N^{1/2}\Omega$. The harmonic-interaction ground state hence has an effective filling factor $\nu = 1$, where $\nu = N(N-1)/2J$ [39]. In [76] FQHE states were observed in large-diameter dots (4000 Å) but not in small-diameter dots (2000 Å). If the height of the confining potential is the same for the two samples, the effective ω_0 for the 2000 Å dot is greater than for the 4000 Å sample. An interpretation in terms of the harmonic-interaction model is hence that the 2000 Å dot satisfies $\omega_0 > N^{1/2}\Omega$ yielding $\nu = 1$, while the 4000 Å dot satisfies $\omega_0 < N^{1/2}\Omega$ yielding $\nu < 1$. [77] has numerically confirmed the fact that the harmonic interaction and the Coulomb interaction do in fact give similar results for sufficiently small parabolic dots (i.e. sufficiently large ω_0).

4.3. 3D quantum dot

Because of the computational complexity, relatively little theoretical work has yet been performed on the effects of the electron–electron interaction in the case of three-dimensional dots ($L_x \sim L_y \sim L_z$) despite the fact that experimental work has already begun [78].

For a three-dimensional isotropic parabolic dot without magnetic field, the $N = 2$ problem is exactly solvable with the inverse-square interaction. The energy is given by $E = E_{CM} + E_{rel}$ where E_{CM} is the energy of a single electron in a 3D parabolic potential

$$E_{CM} = \hbar\omega_0(2n' + l' + \tfrac{3}{2}) \tag{10}$$

and

$$E_{\mathrm{rel}} = \hbar\omega_0(2n + s + 1) \tag{11}$$

where $s = (l(l+1) + m^*\alpha/\hbar^2 + \frac{1}{4})^{1/2}$; l' and l are the centre-of-mass and relative angular-momentum quantum numbers ($l', l \geqslant 0$ and $n', n \geqslant 0$). Extension to finite magnetic fields and/or consideration of larger numbers of electrons is an open problem with the inverse-square model. The only analytically solvable model for N electrons in a 3D dot so far is the harmonic-interaction model. Using this model, it was predicted [66] that the freedom of motion of the electrons in the third (z) direction could lead to dimensional instabilities in the quantum-dot electron gas resulting from the interplay of the electron–electron interaction, the Pauli exclusion principle, the single-particle confinement energy and the cyclotron energy.

5. Energy spectrum of coupled quantum dots

So far we have discussed the energy spectrum of an isolated quantum dot. It is natural to turn to consideration of coupled dots, particularly because future quantum-dot electronic devices may depend on such a coupling for the propagation of information. Coupling between two adjacent dots can be achieved in two ways. First, single-particle tunnelling can occur between the two dots. Alternatively the two-body electron–electron interaction can couple electrons in adjacent dots, even in the absence of any single-particle tunnelling. There have been a number of calculations of the collective modes of arrays of dots in the absence of interdot tunnelling. Kempa *et al* [79] assumed classical point-dipole interactions between the dots and showed that the system could undergo ferroelectric or antiferroelectric transitions. Dempsey *et al* [80] carried out a calculation of polariton modes including retardation effects and generalized the Kohn theorem centre-of-mass absorption to such a dot array. Recently Stafford and Das Sarma [81] have carried out an interesting calculation based on a Hubbard model of the energies of clusters of coupled quantum dots with interdot tunnelling included. Although such a model does not include the subtle dependences of the intradot electron–electron interaction on the magnetic field, it is able to predict a rich phase diagram. Chakraborty *et al* carried out a calculation for two parabolic dots lying alongside each other in the same plane [82]. They found that the interdot electron–electron interaction gives rise to anticrossing behaviour involving the two expected Kohn-theorem far-infrared absorption peaks (the interdot electron–electron interaction breaks the circular symmetry and mixes the centre-of-mass and relative modes of each dot). This anticrossing was found to be consistent with recent experimental data [82].

Tewordt *et al* have recently reported the experimental study of transport through two vertically coupled quantum dots [83] and Bryant has calculated energy spectra numerically in the absence of a magnetic field [84]. The two coupled 2D quantum dots lie in the xy plane but are separated from each other by a vertical distance s along the z-axis. Such a double-layer system could have interesting properties at large axial magnetic field in light of the recent experimental discovery in double-layer electron systems of novel fractional-quantum-Hall-effect (FQHE) states at $\frac{1}{2}$ and $\frac{1}{4}$ filling per layer [85]. In a double-layer system, the ground state should depend on both intralayer and interlayer correlations [86]. The exactly analytically solvable, inverse-square interaction model discussed earlier for $N = 2$ electrons in a dot [58] can be extended to such a double-dot structure. With two electrons in each dot, the model becomes analytically solvable in the limit that the average electron–electron separation within the plane is smaller than the plane separation s, and the interlayer

tunnelling is neglected. Figure 9 shows the low-lying energy spectrum as a function of magnetic field for $s = 391$ Å. The states are labelled as $|m_t, m_b\rangle$ where m_t and m_b are the relative angular momenta of the two electrons in the top and bottom dots respectively. The energies are measured relative to the low-field ground state and successive ground states are labelled. Each state $|m, m\rangle$ with $m_t = m_b = m$ (dashed lines in figure 9) is essentially just the product of two single-dot states (m increases with magnetic field due to the intradot ground-state transitions as discussed in section 4.2); these $|m, m\rangle$ states show no significant interplane correlation and are essentially 'pure' (i.e. weak entanglement). The mixed states $|m+2, m\rangle_-$ (solid lines in figure 9) are a linear combination of equal amounts of $|m+2, m\rangle$ and $|m, m+2\rangle$ (i.e. strong entanglement) and show significant interlayer correlation; their corresponding charge distribution closely resembles the classical electrostatic configuration for four electrons (the electrons lie at the corners of a square when projected onto the xy plane). These mixed states show increasing interplane crystallization with increasing magnetic field and could represent precursors of a bilayer Wigner solid. A s increases (see inset in figure 9) the mixed states (dark regions in inset) become unstable. Eventually all ground states have the pure form $m_t = m_b$ since the interplane correlation is too weak. Intriguingly, the corresponding sequence of effective ground-state filling factors from this few-electron model seems to be consistent with the experimental data [85] obtained in the large-N double-layer electron system [87].

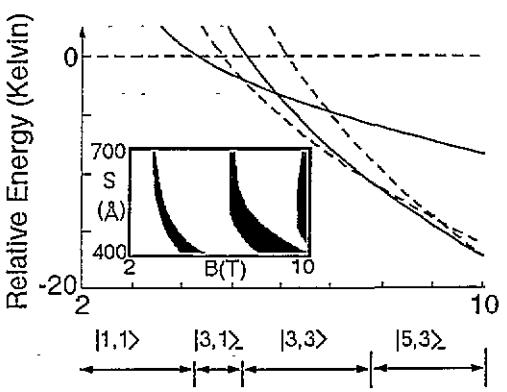

Figure 9. Analytical energy-level spectrum for two coupled ($d = 2$) dots each containing two electrons interacting via the inverse-square interaction, as a function of magnetic field. The dots are parallel and separated vertically by a distance s ($s = 391$ Å as in [85]). Lowest-energy curve at a given B gives ground state. Energies are measured in kelvin relative to $|1, 1\rangle$ (ground state at low magnetic field). Inset shows ranges of stability of the various ground states with increasing s. White regions are pure states $|m, m\rangle$ while dark regions are mixed (entangled) states $|m+2, m\rangle_-$.

There has been much discussion of the possibilities that quantum dots offer as ultrasmall structures within the field of electronics. It is expected that coupled quantum dots could be particularly important in the fabrication of ultrasmall logic gates [88]. Lent and Tougaw have looked at possible geometries for such logic gates; they have proposed a five-dot structure which could form the basis of a cellular automaton [89]. Most suggestions in the literature have been made with conventional (i.e. classical) computing in mind. However a novel application of coupled-dot systems as quantum-mechanical logic gates in the newly formed field of 'quantum computation' [90] has recently been proposed [91, 92]. Quantum computation aims to exploit the specific properties of quantum mechanics to carry out

computations; given the existence of interference and entanglement effects in quantum mechanics, there is the possibility of carrying out massively parallel computations when an appropriate state vector is allowed to evolve in time. Two adjacent dots coupled only by the electron–electron interaction (i.e. 'optical wiring') are excellent candidates for building such quantum logic gates; this is particularly true if each dot behaves as a two-level system since the resulting four-level quantum-dot 'molecule' can be selectively (and reliably) switched between states using external laser pulses [91]. One might expect a pair of 1D quantum dots each containing a single electron would suffice. However the nearly parabolic confining potential in most fabricated quantum dots means that each dot has nearly equispaced energy levels in addition to spin degeneracy. This unfortunately will introduce errors (uncertainties) into the selective switching process. Two 2D dots each containing a single electron at zero magnetic field suffer from a similar problem in that each dot has nearly equispaced levels at both small and large magnetic fields. Given the rich structure of the energy levels in figure 9, and their lack of degeneracy, it seems that two electrons per 2D dot might be more suitable. In addition, the magnetic field provides an externally tunable parameter, enabling one to move between 'pure' and 'entangled' ground states.

Coupled quantum dots might also prove useful for shedding light on some fundamental questions of quantum mechanics. One example is the Fermi two-atom causality problem which, in dot language, relates to two adjacent dots with negligible interdot electron tunnelling. If at time $t = 0$ dot 1 is in an excited state but dot 2 is in the ground state, one can ask the question as to the time t taken for dot 2 to become excited. Originally Fermi had calculated that $t \geqslant s/c$ where c is the speed of light and s is the dot–dot separation; this is consistent with the effects of retardation and hence relativity. However this result has recently been questioned [93]. Subtleties of state entanglement also lie behind other recent propositions such as quantum cryptography and teleportation. Possible realizations of such effects have generally been discussed in terms of photon states. We believe that coupled quantum dots could be good candidates for studying such phenomena in fermion systems.

6. Conclusion

In addition to the technological potential, the study of quantum dots has opened up the fascinating area of few-body quantum mechanics within the traditionally large-N field of condensed-matter physics. Unfortunately, it becomes increasingly difficult experimentally to obtain energy spectra for N-electron dots as $N \rightarrow 1$ while theoretically the reverse is true. However, with improved experimental and theoretical techniques being developed, the next decade should provide a unique opportunity for experimental and theoretical collaboration in this small-N regime. In addition to large-scale numerical calculations, we feel that analytically solvable models of the type discussed here, with effective microscopic parameters that can account for many-body interactions, should prove useful in deducing trends in the large amount of experimental data that is expected to emerge. As a first step in this direction, we have highlighted the extent to which such analytic models can reliably reproduce the physics emerging from (exact) numerical calculations.

Acknowledgments

I am extremely grateful to Luis Quiroga, Simon Benjamin, Richard Haase, Artur Ekert and Pak-Ming Hui for invaluable discussions and collaborations; I also thank the reviewer for very useful comments.

References

[1] See, for example,
1993 *New Sci.* **140** (6 Nov) 21
Drexler K E 1990 *Engines of Creation* (Oxford: Oxford University Press)

[2] See, for example,
Beenakker C W and van Houten H 1991 *Solid State Physics* vol 44, ed H Ehrenreich and D Turnbull (New York: Academic) p 1

[3] Butcher P, March N H and Tosi M P (ed) 1992 *Physics of Low-dimensional Semiconductor Structures* (New York: Plenum)

[4] Heitmann D and Kotthaus J 1993 *Phys. Today* **46** 56

[5] Reed M and Kirk W (ed) 1991 *Nanostructures and Mesoscopic Systems* (San Diego, CA: Academic)
Also see articles contained in the special issue of *Physics Today*:
1993 *Phys. Today* **46**

[6] Chakraborty T 1992 *Comment. Condens. Matter Phys.* **16** 35

[7] Kastner M A 1993 *Phys. Today* **46** 24; 1992 *Rev. Mod. Phys.* **64** 849
Meirav U, Kastner M A and Wind S J 1990 *Phys. Rev. Lett.* **65** 771

[8] Drexler K E 1992 *Nanosystems* (New York: Wiley)

[9] Yoffe A 1995 *Adv. Phys.* at press

[10] Zrenner A, Butov L V, Hagn M, Abstreiter G, Bohm G and Weimann G 1994 *Phys. Rev. Lett.* **72** 3382

[11] Crommie M F, Lutz C P and Eigler D M 1993 *Science* **262** 218

[12] Field M, Smith C G, Pepper M, Ritchie D A, Frost J E F, Jones G A and Hasko D G 1993 *Phys. Rev. Lett.* **70** 1311

[13] McEuen P L, Foxman E B, Meirav U, Kastner M A, Meir Y, Wingreen N S and Wind S J 1991 *Phys. Rev. Lett.* **66** 1926 ,

[14] Johnson A T, Kouwenhoven L P, de Jong W, Van der Vaart N C, Harmans C J M P and Foxon C T 1992 *Phys. Rev. Lett.* **69** 1592

[15] Ford C J B, Simpson P J, Pepper M, Kern D, Frost J E F, Ritchie D A and Jones G A C 1993 *Nanostruct. Mater.* **3** 283

[16] McEuen P L, Foxman E B, Kinaret J, Meirav U, Kastner M A, Wingreen N S and Wind S J 1992 *Phys. Rev.* B **45** 11 419

[17] Sikorski C and Merkt U 1989 *Phys. Rev. Lett.* **62** 2164

[18] Tewordt M, Law V, Kelly M, Newbury R, Pepper M, Peacock D, Frost J, Ritchie D and Jones G 1990 *J. Phys.: Condens. Matter* **2** 8969

[19] Bird J P, Ishibashi K, Stopa M, Taylor R P, Aoyagi Y and Sugano T 1994 *Phys. Rev.* B **49** 11 488; *Solid-State Electron.* **37** 709

[20] See,
Marcus C, Rimberg A J, Westervelt R M, Hopkins P F and Gossard A C 1992 *Phys. Rev. Lett.* **69** 506
for an investigation of quantum chaos in large dots.

[21] Sotomayor Torres C M, Smart A P, Watt M, Foad M A, Tsutsui K and Wilkinson C D W 1994 *J. Electron. Mater.* **23** 289

[22] Nicholls J T, Frost J E F, Pepper M, Ritchie D A, Grimshaw M P and Jones G A C 1993 *Phys. Rev.* B **48** 8866

[23] See
Averin D V and Likharev K K, in 1991 *Mesoscopic Phenomena in Solids* ed B L Al'tshuler, P A Lee and R A Webb (Amsterdam: Elsevier) p 173

[24] Beenakker C W J 1991 *Phys. Rev.* B **44** 1646

[25] Ashoori R C, Stormer H L, Weiner J S, Pfeiffer L N, Baldwin K W and West K W 1993 *Phys. Rev. Lett.* **71** 613; 1992 *Phys. Rev. Lett.* **68** 3088

[26] Meurer B, Heitmann D and Ploog K 1992 *Phys. Rev. Lett.* **68** 1371

[27] Su B, Goldman V J and Cunningham J E 1992 *Phys. Rev.* B **46** 7644

[28] Tewordt M, Law V J, Nicholls J T, Martin-Moreno L, Ritchie D A, Kelly M J, Pepper M, Frost J E F, Newbury R and Jones G A C 1994 *Solid-State Electron.* **37** 793

[29] Bryant G W 1987 *Phys. Rev. Lett.* **59** 1140

[30] We ignore the effect of spin–orbit coupling which can be shown to be small.

[31] Kohn W 1961 *Phys. Rev.* **123** 1242

[32] Brey L, Johnson N F and Halperin B I 1989 *Phys. Rev.* B **40** 10 647

[33] Maksym P A and Chakraborty T 1990 *Phys. Rev. Lett.* **65** 108

[34] Peeters F M 1990 *Phys. Rev.* B **42** 1486

[35] Li Q P, Karrai K, Yip S K, Das Sarma S and Drew H D 1991 *Phys. Rev.* B **43** 5151
[36] Brey L, Johnson N F, Dempsey J and Halperin B I 1990 *Proc. NATO Adv. Res. Workshop on Light Scattering in Semiconductor Structures and Superlattices (Mont Tremblant, 1990)* (New York: Plenum)
[37] Palacios J J, Martin-Moreno L and Tejedor C 1993 *Europhys. Lett.* **23** 495
[38] Laughlin R B 1983 *Phys. Rev.* B **27** 3383
[39] Girvin S M and Jach T 1983 *Phys. Rev.* B **28** 4506
[40] Maksym P A 1993 *Physica* B **184** 386
[41] See also the Monte Carlo calculations of
Bolton F and Rossler U 1993 *Superlatt. Microstruct.* **13** 140
Bolton F 1994 *Phys. Rev. Lett.* **73** 158
[42] Maksym P and Chakraborty T 1992 *Phys. Rev.* B **45** 1947
[43] Wagner M, Merkt U and Chaplik A V 1992 *Phys. Rev.* B **45** 1951
[44] Hawrylak P and Pfannkuche D 1993 *Phys. Rev. Lett.* **70** 485
[45] Hawrylak P 1993 *Phys. Rev. Lett.* **71** 3347
[46] Yang S R E, MacDonald A H and Johnson M D 1993 *Phys. Rev. Lett.* **71** 3194
[47] MacDonald A H and Johnson M D 1993 *Phys. Rev. Lett.* **70** 3107
[48] Kinaret J M, Meir Y, Wingreen N S, Lee P and Wen X G 1992 *Phys. Rev.* B **46** 4681
[49] Bryant G W 1987 *Phys. Rev. Lett.* **59** 1140
[50] Hausler W and Kramer B 1993 *Phys. Rev.* B **47** 16 353
Jauregui K, Hausler W and Kramer B 1993 *Europhys. Lett.* **24** 581
[51] Chui S T 1986 *Phys. Rev. Lett.* **56** 2395
[52] Timp G, Behringer R, Cunningham J E and Howard R E 1989 *Phys. Rev. Lett.* **63** 2268
[53] Kumar A, Laux S E and Stern F 1990 *Phys. Rev.* B **42** 5166
[54] Gudmundsson V and Gerhardts R R 1991 *Phys. Rev.* B **43** 12 098
[55] Pfannkuche D, Gudmundsson V and Maksym P A 1993 *Phys. Rev.* B **47** 2244
[56] Johnson N F and Reina M 1992 *J. Phys.: Condens. Matter* **4** L623
[57] Taut S 1994 *J. Phys. A: Math. Gen.* **27** 1045
[58] Quiroga L, Ardila D and Johnson N F 1993 *Solid State Commun.* **86** 775
[59] Johnson N F and Quiroga L 1994 *Solid State Commun.* **89** 661
[60] Calogero F 1971 *J. Math. Phys.* **12** 419
[61] Johnson N F and Payne M C 1993 *Phys. Rev. Lett.* **70** 1513, 3523
[62] Johnson N F and Payne M C 1991 *Phys. Rev. Lett.* **67** 1157
[63] Que W 1992 *Solid State Commun.* **81** 721
[64] Johnson N F 1992 *Phys. Rev.* B **46** 2636
[65] Johnson N F and Payne M C 1992 *Phys. Rev.* B **45** 3819; 1992 *Superlatt. Microstruct.* **11** 309
[66] Johnson N F 1992 *J. Phys.: Condens. Matter* **4** L555
[67] Moshinsky M 1968 *Group Theory and the Many Body Problem* (New York: Gordon and Breach)
[68] Haase R W and Johnson N F 1993 *Phys. Rev.* B **48** 1583
[69] Haase R W and Johnson N F 1994 *Phys. Rev.* B **49** 14 409
[70] Pfannkuche D and Gerhardts R R 1991 *Phys. Rev.* B **44** 13 132
[71] See, for example, a forthcoming review by
Kawakami N 1995 *Prog. Theor. Phys.* **91** 189
[72] Simons B D, Lee P A and Altshuler B L 1994 *Phys. Rev. Lett.* **72** 64
[73] Ivanov A L and Haug H 1993 *Phys. Rev. Lett.* **71** 3182
[74] Fock V 1926 *Z. Phys.* **47** 446
Darwin C G 1930 *Proc. Camb. Phil. Soc.* **27** 86
[75] Merkt U, Huser J and Wagner M 1991 *Phys. Rev.* B **43** 7320
[76] Hansen W, Smith T P, Lee K Y, Hong J M and Knoedler C M 1990 *Appl. Phys. Lett.* **56** 168
[77] Johnson B L and Kirczenow G 1993 *Phys. Rev.* B **47** 10563
[78] Meurer B, Heitmann D and Ploog K 1993 *Phys. Rev.* B **48** 11 488
[79] Kempa K, Broido D A and Bakshi P 1991 *Phys. Rev.* B **43** 9343
[80] Dempsey J, Johnson N F, Brey L and Halperin B I 1990 *Phys. Rev.* B **42** 11708
[81] Stafford C A and Das Sarma S 1994 *Phys. Rev. Lett.* **72** 3590
[82] Chakraborty T, Halonen V and Pietilainen P 1991 *Phys. Rev.* B **43** 14 289
[83] Tewordt M, Hughes R J F, Martin-Moreno L, Nicholls J T, Asahi H, Kelly M J, Law V J, Ritchie D A, Frost J E F, Jones G A C and Pepper M 1994 *Phys. Rev.* B **49** 8071
[84] Bryant G W 1993 *Phys. Rev.* B **48** 8024
[85] Eisenstein J P, Boebinger G S, Pfeiffer L N, West K W and He S 1992 *Phys. Rev. Lett.* **68** 1383
[86] He S, Xie X C, Das Sarma S, Zhang F C 1991 *Phys. Rev.* B **43** 9339.

Yang K, Moon K, Zheng L, MacDonald A H, Girvin S M, Yoshioka D and Zhang S C 1994 *Phys. Rev. Lett.* **72** 732

[87] Benjamin S and Johnson N F 1995 unpublished

[88] Teich W G, Obermayer K and Mahler G 1988 *Phys. Rev.* B **37** 8111

[89] Lent C and Tougaw P D 1993 *J. Appl. Phys.* **74** 6227

[90] Deutsch D 1992 *Phys. World* **5** (June) 57

[91] Mahler G and Ekert A K unpublished
Paz J P and Mahler G 1993 *Phys. Rev. Lett.* **71** 3235

[92] Penrose R 1994 *Shadows of the Mind* (Oxford: Oxford University Press)
Penrose suggests that quantum computation may occur within the brain. Microtubules in each neuron contain arrays of coupled tubulins which appear similar to coupled dots.

[93] Hegerfeldt G C *Phys. Rev. Lett.* **72** 596